Applied Catalysis B: Environmental 244 (2019) 56–62

Contents lists available at ScienceDirect

Applied Catalysis B: Environmental

journal homepage: www.elsevier.com/locate/apcatb

Self-assembled Cu-Ni bimetal oxide 3D in-plane epitaxial structures for highly efficient oxygen evolution reaction

Chaojiang Li[a,b], Bowei Zhang[a,*], Yong Li[b], Shiji Hao[a], Xun Cao[a], Guang Yang[a], Junsheng Wu[d,**], Yizhong Huang[a,c,*]

[a] School of Materials science and Engineering, Nanyang Technological University, 50 Nanyang Avenue, 639798, Singapore
[b] Department of Mechanical Engineering, Beijing Key Lab of Precision / Ultra-precision Manufacturing Equipments and Control, Tsinghua University, Beijing 100084, China
[c] College of Science, Hubei University of Technology, Hongshan District, Wuhan, 430068, China
[d] Institute of Advanced Materials and Technology, University of Science and Technology Beijing, Beijing, 100083, China

ARTICLE INFO

Keywords:
Electrochemistry
Oxygen evolution reaction
Liquid plasma discharge
3D porous electrode

ABSTRACT

To improve the catalytic activity of copper based electrode for oxygen evolution reaction (OER), double cathodes liquid plasma discharge (DC-LPD) method was developed to fabricate three-dimensional (3D) nest-like structures electrode on the nickel foam (NF). The CuO-NiO/NF electrode obtained through annealing the in-plane epitaxial $Cu(OH)_2$-Ni_2O_3H/NF in the oven, exhibits excellent electrocatalytic activities for the oxygen evolution reaction at a low overpotential of 319 mV to achieve a current density of 10 mA/cm^2. The electrochemically active surface area (ECSA) of CuO-NiO/NF is over 2 times larger than that of $Cu(OH)_2$-Ni_2O_3H/NF electrode. The synergistic effort between Cu and Ni makes the CuO-NiO/NF electrode a superior electrocatalyst with improved activity and stability as compared to the single NiO/NF electrode.

1. Introduction

Electrochemical splitting of water to produce oxygen (O_2) through an anodic oxygen evolution reaction (OER) is one of the most appealing strategies for the storage of renewable energies [1–4]. At present, IrO_2 and RuO_2, are considered as the state-of-the-art catalysts for OER [5–9], but their scarcity and high cost significantly hamper their practical applications. As a result, the development of high-efficient catalysts with economical materials is being paid extensive attention [10–12].

Over the past decade, significant advances have been achieved in developing OER catalysts based on the first-row transition metals [13–17]. Especially, there has been increasing interest in copper based water oxidation catalysts due to their high abundance, low cost and rich redox properties [18–24]. The copper based electrocatalyst materials were typically prepared by electrodeposition, solid-state reaction or hydrothermal reaction followed by cast as an extraneous layer onto electrode substrate surfaces using electrical insulating binding agents such as Nafion [25–27]. These fabrication procedures need several steps which increase the cost for catalyst preparation and decrease catalyst performance stability. Furthermore, most of the reported copper based electrocatalysts have an over potential of more than 400 mV for the OER, which is much higher than that of the well-studied nickel or cobalt-based composites [20,28,29]. The improvement in the OER performance of copper-based catalysts is still highly desirable and challenging.

Liquid plasma discharge (LPD), as one of the advanced oxidation processes (AOPs), is a powerful discharge process where the plasma is generated in the interface of the cathode electrode and the electrolytic solution, which has been demonstrated to initiate a variety of chemical and physical effects [30–32]. In the traditional liquid plasma discharge process, only one cathode is used to synthesize various nano-particles or nano-wires for electro-catalysis [33–35], but it is difficult to fabricate three-dimensional (3D) structures.

3D structures electrodes maintaining a large surface-area-to-volume ratio can help to accommodate more catalytically active sites [16,36–38]. Meanwhile, a binary copper based catalyst has superior OER activities as compared to those of single copper oxides [24]. Hence, with the aim of lowering the overpotential of OER for copper based catalyst, a novel self-assembly method of double cathodes liquid plasma discharge (DC-LPD) was proposed and aimed to efficiently fabricate three-dimensional (3D) structures electrode on the nickel foam (NF) substrate. As such, four different catalytic electrodes (Cu

* Corresponding author at: School of Materials science and Engineering, Nanyang Technological University, 50 Nanyang Avenue, 639798, Singapore.
** Corresponding author.
E-mail addresses: bzhang011@e.ntu.edu.sg (B. Zhang), wujs76@163.com (J. Wu), YZHuang@ntu.edu.sg (Y. Huang).

https://doi.org/10.1016/j.apcatb.2018.11.046
Received 30 July 2018; Received in revised form 14 November 2018; Accepted 16 November 2018
Available online 16 November 2018

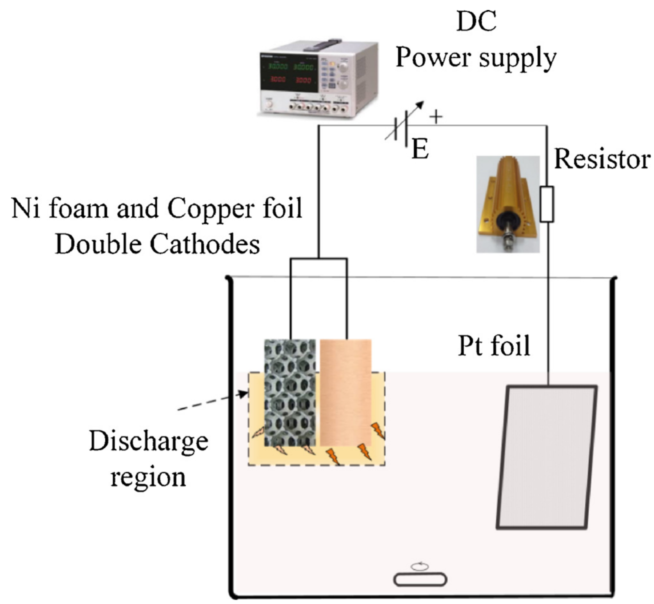

Fig. 1. Schematic of $Cu(OH)_2$-Ni_2O_3H/NF electrode fabrication using double cathodes liquid plasma discharge.

$(OH)_2$-Ni_2O_3H/NF, CuO-NiO/NF, NiO/NF and bare NF were selected and examined in terms of their catalytic performance to oxygen evolution reaction.

2. Experimental section

2.1. Fabrication of copper based electrodes

Preparation copper based nickel foam (NF) electrodes: $Cu(OH)_2$-Ni_2O_3H/NF was prepared according to the liquid plasma method of double cathodes, where the thickness of 0.15 mm Cu foil and 0.2 mm Ni foam were used as cathode and a platinum foil (30 mm × 10 mm × 1 mm, 99.9% purity) as the anode in the 2 M NaOH electrolyte solution. Various active species, such as •OH radicals, •H radicals, H_2O_2, and hydrated electrons [39], were generated in the plasma zone of cathodes by connecting to a direct current (DC) power supply (70 V, 0.8 A), as seen in Fig.1. Before plasma discharge, the Cu foil and Ni foam were washed with dilute hydrochloric acid and deionized (DI) water several times to remove surface impurities and oxide layer. After about 5 min of plasma discharge, the Ni foam cathode was taken out from the electrolyte solution. It was found that the color of NF changed slowly from red to light blue. The obtained $Cu(OH)_2$-Ni_2O_3H/NF electrode was dried at 160 °C, for 2 h in the oven. $Cu(OH)_2$-Ni_2O_3H was then dehydrated and transformed into bimetal oxide (i.e. CuO-NiO). For comparison, NiO/NF electrode was prepared by traditional single cathode liquid plasma method.

2.2. Characterization of catalysts

The crystallinity and phases of the samples were characterized using an X-ray diffractometer (XRD, Bruker, AXS D8) under spin mode operating at 40 kV and 40 mA and scanned at the rate of 2°per min within the range of 10° ≤ 2θ ≤ 80°. The morphology and internal structure of the samples were further examined by using field emission scanning electron microscope (FESEM, JEOL JSM-7600 F). High-resolution transmission electron microscopy (HR-TEM) and selected area electron diffraction (SAED) patterns of the samples were characterized using a field-emission transmission electron microscope (FE-TEM, JEM-2100 F, JEOL, Japan), which was operated at an accelerating voltage of 200 kV. The elemental compositions were determined by energy dispersive X-ray spectroscopy (EDS) using the genesis microanalysis system (EDAX) attached to the TEM. X-ray photoelectron spectroscopy (XPS) for elemental analysis was conducted on a Kratos Axis Ultra DLD X-ray photoelectron spectrometer.

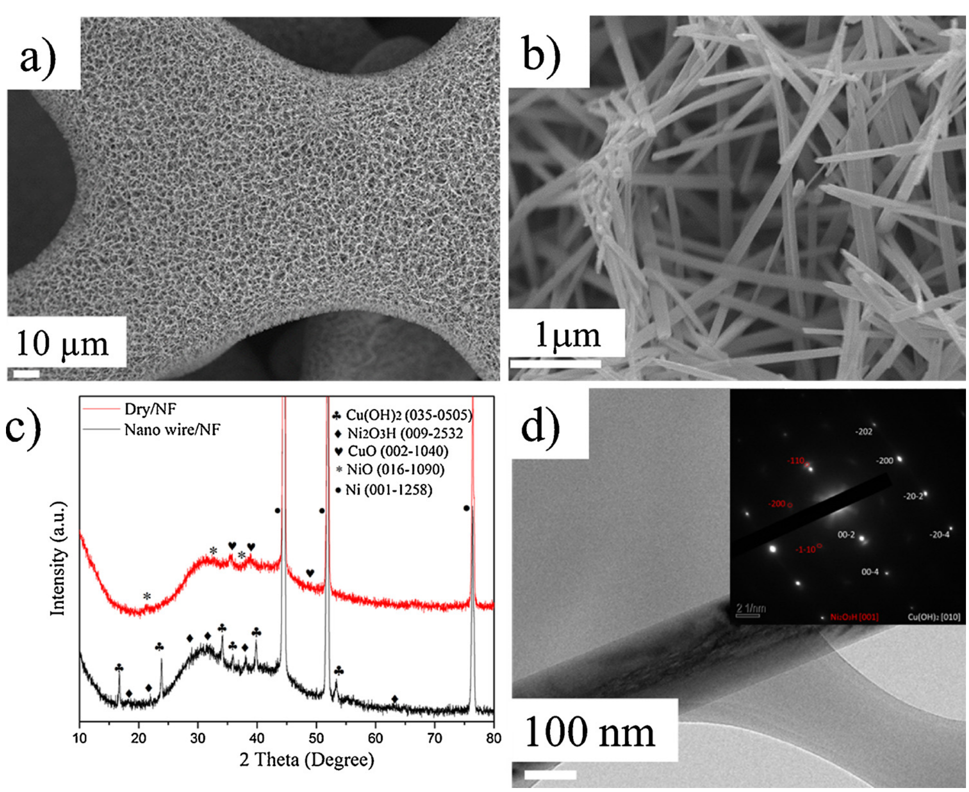

Fig. 2. a) and b) SEM images of Nano wire/NF; c) XRD patterns; d) TEM image and SAED image of Nano wire /NF.

3. Results and discussion

3.1. Catalysts characterization of SEM, TEM, XRD, EDS and XPS

The surface of Ni foam electrode was viewed in SEM after subjected to double cathode liquid plasma discharge and appears 3D nest-like structure (Fig. 2a and Fig. s1), as the consequence of H_2 bubbles generated and dissipated during cathode discharge process of the Ni foam substrate. These nests are seen to be formed by a number of homogeneous nano-wires at a higher magnification as shown in Fig. 2b, with the diameter and length of nanowires estimated to be approximately 180 nm and 20 μm, respectively. These nano-wires consist of two compositional phases (i.e. $Cu(OH)_2$ and Ni_2O_3H) as identified from X-ray diffraction (XRD) pattern (Fig. 2c). In fact, the color of the sample was found to change from red to black after the exposure in air for 20 min at room temperature (Fig. s2), which indicates the compositional or structural transformation as a consequence of the energy release of particles on the NF surface. The presence of these two phases is further confirmed from Fig. 2d through indexing the inset selected area diffraction (SAD) pattern collected from the nanowire. The pattern consists of two sets of diffraction spot arrays. The strong intensity diffraction spot array is reflected from $Cu(OH)_2$ lattice and the weak intensity spot array is generated from Ni_2O_3H. The strong pattern represents the reciprocal lattice of $Cu(OH)_2$ and the weak pattern does the reciprocal lattice of Ni_2O_3H oriented at the zone axis of [0 1 0] and [0 0 1], respectively. Both phases are epitaxial in the {0 0 2} lattice plane, which suggests the coplanar growth of $Cu(OH)_2$ and Ni_2O_3H. These results are further proven from the high-resolution TEM image (Fig. s3). It is worth to note that both $Cu(OH)_2$ and Ni_2O_3H are completely coherent in all lattice orientations but uniformly distributed across the single nano-wires based on the energy dispersive X-ray spectroscopy (EDS) (Fig. s4).

X-ray photoelectron spectroscopy (XPS) was performed to further clarify the phase structures of $Cu(OH)_2$-Ni_2O_3H/NF (Nano wire /NF). As usual, the calibration was made by using the C 1 s peak (284.6 eV). The wide-scan XPS spectrum shows that the electrode surface contains a range of elements O, Ni, Cu as shown in Fig. 3. In the O 1 s XPS spectrum, the binding energies at 529.8 and 531.5 eV can be ascribed to the respective O^{2-} and OH- from Ni_2O_3H and $Cu(OH)_2$ [29,40], in agreement with the XRD results. In the Cu 2p spectra, typical Cu 2p3/2 peaks are observed with binding energies of 933.8 eV, whilst their associated shakeup peaks at 941.2 and 943.2 eV are also visible. These Cu 2p peaks are consistent with previous studies of $Cu(OH)_2$ [41]. The binding energy of Ni 2p3/2 can be fitted well by three peaks located at 852.6, 855.7 and 857.9 eV, which can be attributed to metallic state Ni, Ni^{2+} and Ni^{3+}, respectively [12], indicating the formation of Ni_2O_3H on the nickel foam.

The synthesized nanowires were carried out with annealing in oven at the temperature of 160 °C for 2 h. Fig. 4a shows the morphology of the annealed nano-wires, where the tips of nano-wires become bent or curved due to intramolecular dehydration of the as-obtained hydroxide species. The implementation of XRD pattern generated from the annealed products (Fig. 2c) suggests that hydrated Cu and Ni oxides were completely transformed into pure CuO and NiO. The inset (down) in Fig. 4a is the selected area electron diffraction (SAED) patterns taken from the bright-field TEM image (the inset (upper) of Fig. 4a). Fig. 4b is the high-resolution TEM image of nano-wire after annealing. Likewise, there are two sets of diffraction spot array visible with one generated from CuO and the other from NiO as shown the inset of Fig. 4b. These results are further claimed from the high-resolution XPS spectra of Ni 2p, Cu 2p and O 1 s (Fig. 4c - e), where Ni 2p and O 1 s are different from the Fig. 3d and 3 b. In the Ni 2p spectra, typical Ni 2p3/2 peaks are only observed with the respective binding energies of 852.6 eV and 853.7 eV. The binding energy values at 529.4 eV and 531.4 eV are associated with O^{2-} species in the lattice and oxygen vacancies or defects [42]. These Cu 2p peaks (933.8 eV) are attributed to CuO. Based on the XPS and EDS (Fig. s5), the content of copper element is over six times larger than that of nickel element. Some cracks are found on the surface of dry nanowires ascribed to the intramolecular dehydration at a higher temperature oven for long time, which is identical to morphology in Fig.4a. The NiO/NF electrode is fabricated with nickel foam as single cathode by the traditional liquid plasma discharge method (Fig. s6). Compared to bare NF (Fig. s7), and the surface of NiO/NF are witnessed to covering with some rods compared to bare NF.

Fig. s8 presents the isothermal plot of nitrogen adsorption/desorption of the electrode with a clear H3 hysteresis loop between adsorption/desorption, which is characteristic for porous structure material. The porous CuO-NiO/NF and $Cu(OH)_2$-Ni_2O_3H/NF electrodes exhibit the Brunauer– Emmett–Teller (BET) surface area of 51.4 $m^2 g^{-1}$, 32.6 $m^2 g^{-1}$, respectively. The corresponding Barrett-Joyner-Halenda (BJH) pore size distribution is exhibited in the inset of the image, suggesting that the pore sizes of the CuO-NiO/NF and $Cu(OH)_2$-Ni_2O_3H/NF electrodes are around 41.5 and 46.3 nm, respectively, which are well in accordance with the SEM results. The existence of mesoporous nature and high BET specific surface area of the as-prepared sample provide low-resistance pathways and offer more active sites for OER [43,44].

3.2. OER catalytic performances

Fig. 5a shows the LSV plots of the Cu-Ni dual cathodes (i.e.$Cu(OH)_2$ - Ni_2O_3H/NF, CuO-NiO/NF) and the Ni single cathodes (i.e. NiO/NF and the bare nickel foam (NF)) for OER in 1 M NaOH solution. In contrast, the CuO-NiO/NF electrode exhibits significantly enhanced catalytic activity with a smaller overpotential η of 319 mV that drives the current density of 10 mA/cm^2, which is lower than that of commercial IrO_2 (325 mV). As shown in table s1, this overpotential η for CuO-NiO/NF is lower than the previously reported copper based OER catalysts in alkaline conditions. Meanwhile, to obtain the current density of 10 mA/cm^2 for $Cu(OH)_2$- Ni_2O_3H/NF electrode, an overpotential η of 370 mV is required, which is slightly higher than CuO-NiO/NF. But both of them are far lower than the bare NF. It is believed that the coplanar growth of Cu and Ni oxides gives rise to a number of interfaces. These interfaces are not fully epitaxial due to the different lattice plane spaces and contain a lot of defects, which will provide effective paths that allow the fast transportation of chargers. The NiO/NF electrode fabricated with nickel foam as single cathode by liquid plasma discharge method had also lower overpotential than the bare NF, implying that the nano-rods (Fig. s6.b) on the surface of NiO/NF can improve the catalytic activity. An apparent anodic peak before the catalytic OER onset is visible in the LSV of all electrodes consistent with conversion of incorporated divalent Ni to/from trivalent Ni in the alkaline solution [14].

In order to avoid the oxidation peak, Tafel plot was obtained based on the cathodic sweep curve (Fig.s9). Fig. 5b shows the respective Tafel plots of four electrodes where $Cu(OH)_2$-Ni_2O_3H/NF electrode was measured to have a Tafel slope of 93.6 mV/dec, which is higher than CuO-NiO/NF electrode with the slope value of 86.4 mV/dec. Pure Cu and Ni oxides have kinetic more favorable to implement catalytic activity than hydrated Cu and Ni oxides. They both are better than the bare NF. This result is further confirmed by electrochemical impedance spectroscopy (EIS) (Fig. 5c) analysis in that the $Cu(OH)_2$-Ni_2O_3H/NF and CuO-NiO/NF have much lower electrical resistances than Ni oxide and bare Ni. Additionally, the long-term durability is another critical parameter that is of great significance for practical energy conversion and storage. The controlled potential electrolysis experiment demonstrates that the CuO-NiO/NF electrode can maintain a current density of about 15 mA/cm^2 at 1.61 V versus RHE for at least 10 h (Fig. 5d), indicating its excellent long-term durability in strong basic media. After long time stability test, the surface structure remains intact (Fig. s10). As compared with fresh electrocatalyst, the peak position of Cu^{2+} shifts positively (Fig. s10d), which may be due to the occurrence of surface

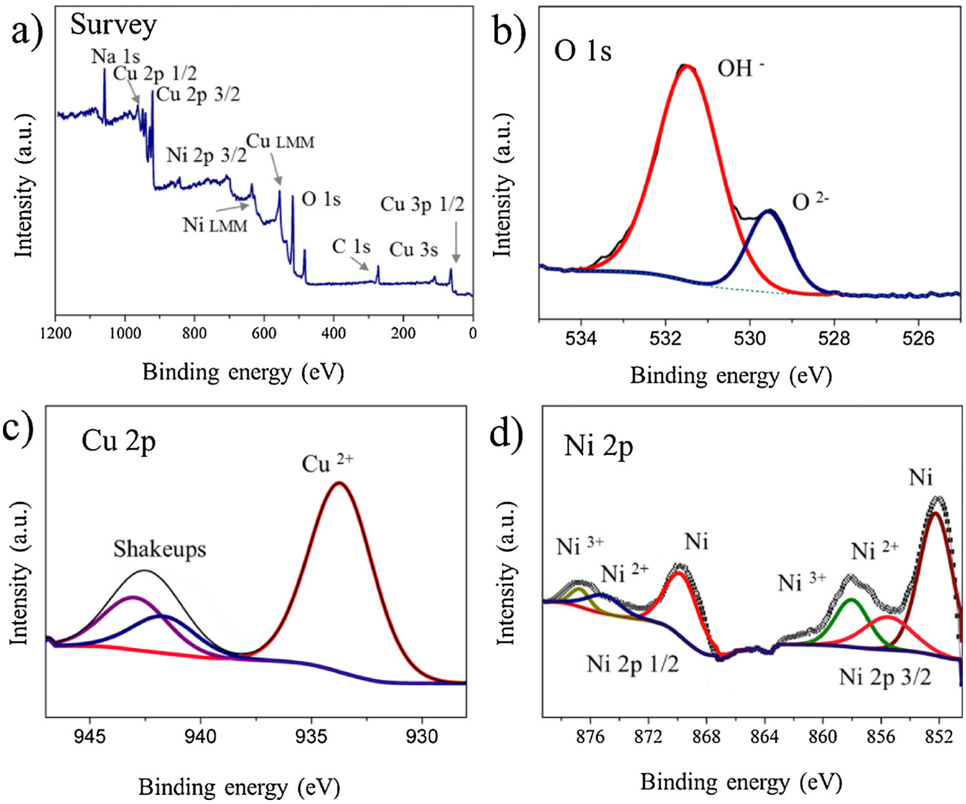

Fig. 3. XPS analysis of $Cu(OH)_2/Ni_2O_3H$ electrode, a) XPS survey and high-resolution XPS spectra of O 1 s (b), Cu 2p (c), and Ni 2p (d).

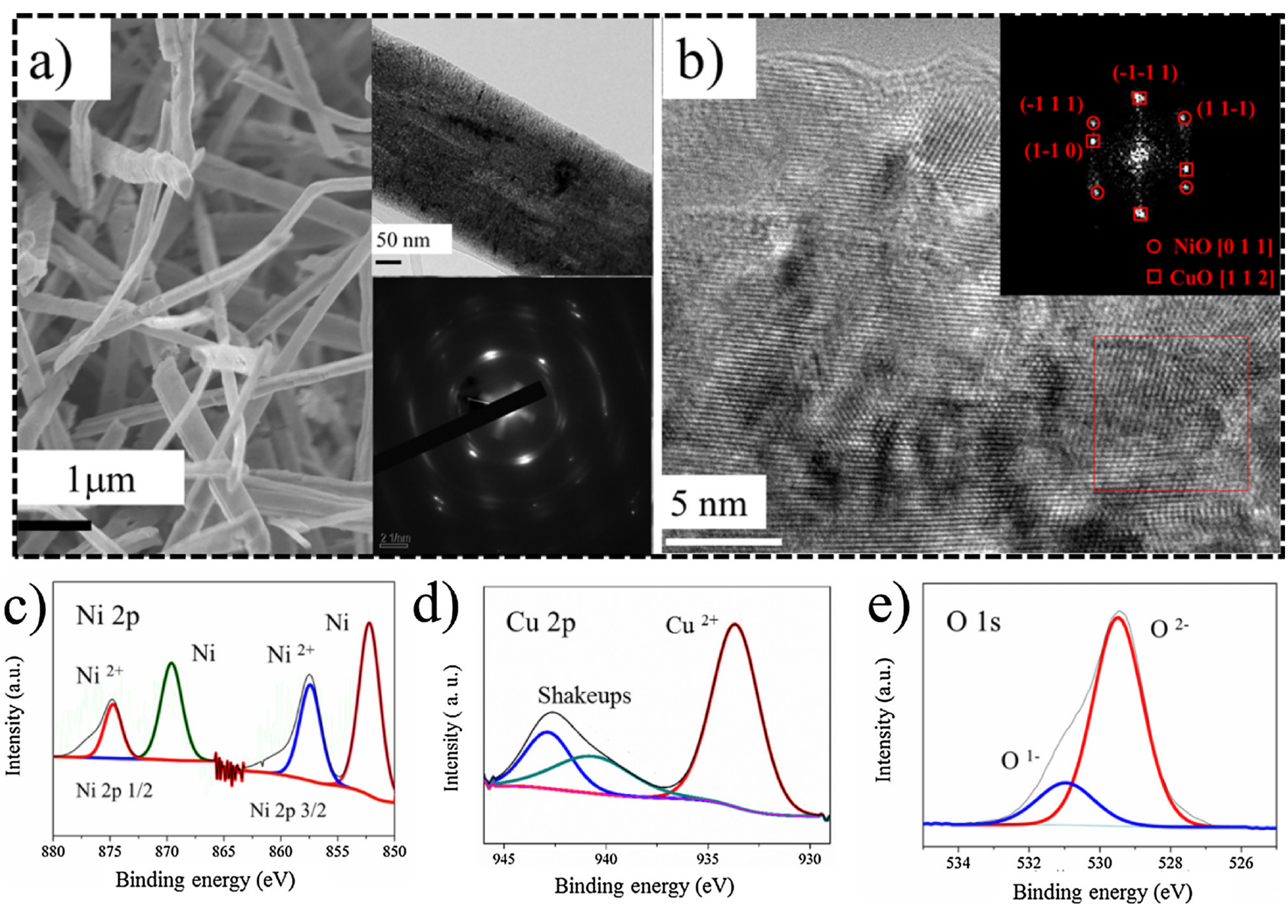

Fig. 4. a) SEM image of annealed nano-wires and their TEM image(upper inset) and SAED (down inset),b) high-resolution TEM and FFT image (inset), the high-resolution XPS spectra of Ni 2p (c), Cu 2p (d) and O 1 s (e).

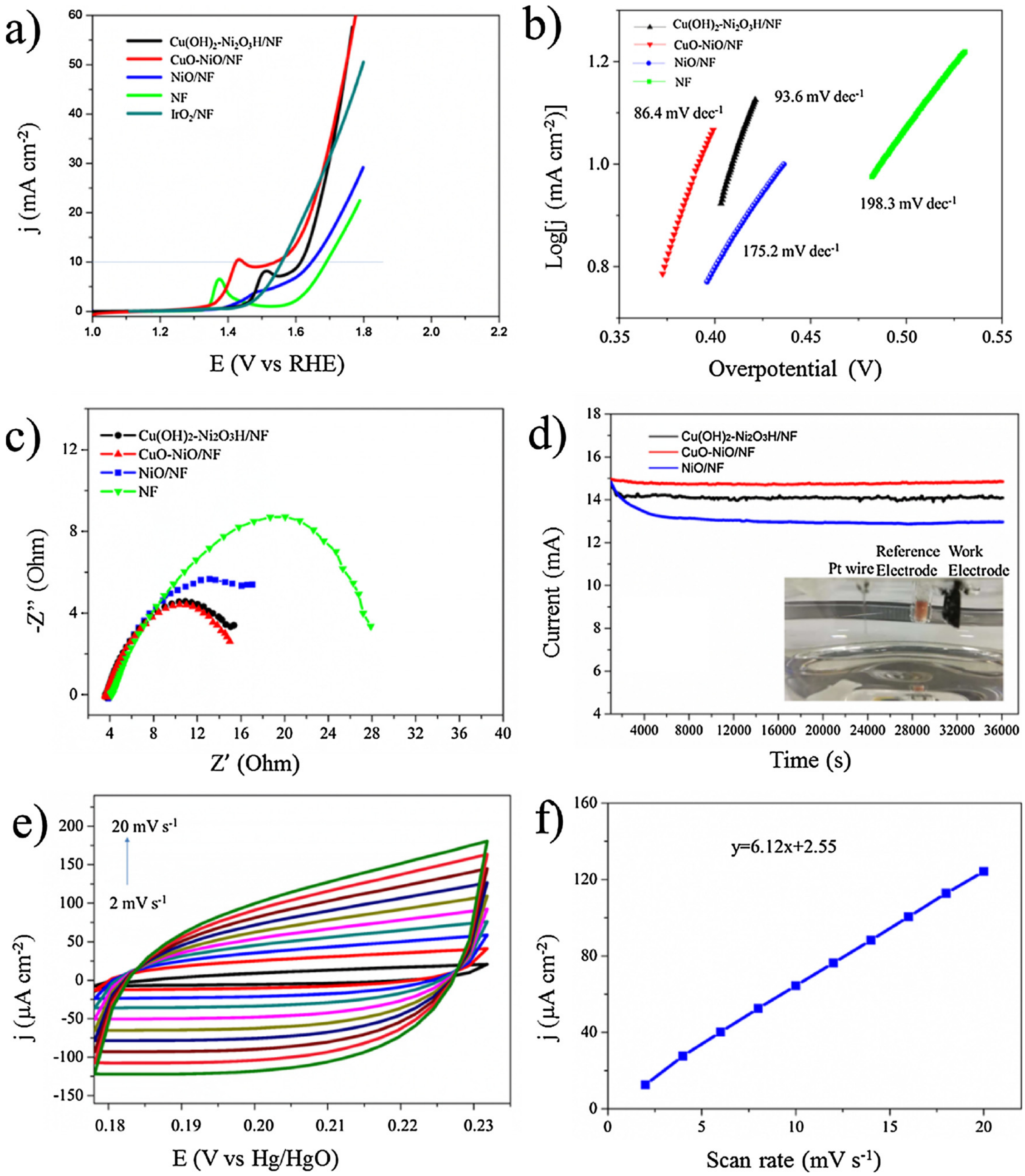

Fig. 5. OER catalytic performances of four different electrodes in 1 M NaOH electrolyte without iR-compensation. a) LSV scan curves using a scan rate of 5 mV/s, b) Tafel plots, c) Nyquist plots from 1 MHz to 0.01 Hz at an applied potential of 1.58 V vs. RHE. d) Chronoamperometric curve at an applied potential (corresponding 15 mA) e)-f) Capacitative charging currents of the CuO-NiO/NF electrode recorded in the non-Faradaic potential region at scan rates from 2 to 20 mV/s at an interval of 2 mV.

electron reorganization during OER process [45]. The LSV and EIS were also tested after the stability test (Fig. s11). The low overpotential shift of LSV and EIS curves confirm the stability of CuO-NiO/NF electrode. Furthermore, the turnover frequency (TOF) of the catalyst was also calculated (see support information for details of the TOF calculations). The calculated TOF values at 10 mA/cm^2 for CuO-NiO/NF and Cu$(OH)_2$-Ni_2O_3H/NF are 0.3977 and 0.163 s^{-1}, respectively, reflecting highly active catalyst compared with the NiO/NF (TOF,0.133 s^{-1}).

The electrochemically active surface area (ECSA) is estimated by cyclic voltammetry (CV) on the basis of the double-layer capacitance (C_{dl}) of the materials, as shown in Fig. 5e, f and Fig. s12-14. The CVs in the non-Faradaic potential region were recorded at a series of scan rates from 2 to 20 mV/s with an interval of 2 mV. The C_{dl} and ECSA of the Cu$(OH)_2$-Ni_2O_3H/NF electrode are calculated to be 2.52 m F/cm^2 and 63 cm^2, respectively. Meanwhile, the corresponding C_{dl} and ECSA of the CuO-NiO/NF electrode are calculated to be 6.12 m F/cm^2 and 153 cm^2. Both electrodes are far higher than the bare NF (15.12 cm^2). Such a large ECSA is of great help for the enhancement of the catalytic activity for the OER. According to above OER catalytic performances, the results show that the 3D nest- like structure electrodes prepared by double cathodes of NF and copper foil are highly active compared to the bare NF and the NiO/NF electrode fabricated by the single cathodes discharge, due to their high electrochemical surface areas with efficient electron/ion transport and bubble migration.

3.3. Effects of the DC-LPD on the fabrication of catalysts

Owing to the Joule heat, partial melting and gasification may occur

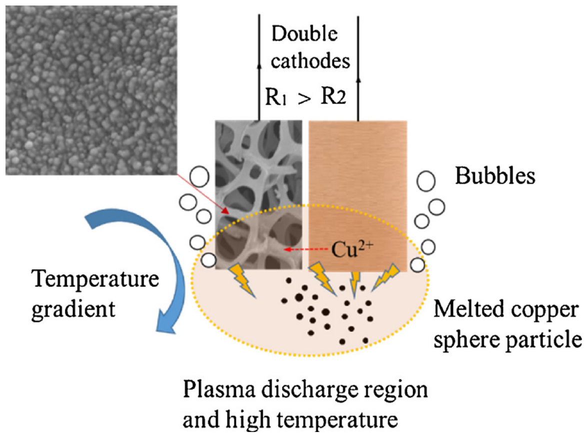

Fig. 6. The particles fabrication mechanism of DC-LPD.

at the solid-liquid interface, where gas bubbles are generated. When the voltage is sufficiently high and reaches the value of threshold voltage, the cathode will be entirely isolated from the solution by the gas bubbles, leading to the initiation of plasma discharge at the interface between the cathode and the electrolytic solution [33]. In the applied electric field, the cations in the plasma bombard the cathode and result in a sputtering event. Under the effect of the plasma in water-based solution, large number of electrons, free radicals, hydronium cations (H_3O^+) and hydrogen peroxide (H_2O_2) [46] are formed, which are strong oxidizing agents [39,46].

$$H_2O \overset{plasma}{\rightarrow} e^-_{aq},\ \bullet H,\ \bullet OH,\ H_2,\ H_2O_2,\ H_3O^+$$

The synthesis of nanowires follows the solid-liquid-solid growth model. Fig. 6 illustrates that the double cathodes liquid plasma discharge is an electrochemical physical process in a high temperature, which involves electrochemical deposition process and physical sputtering process.

Electrochemical deposition process: The two cathodes (Ni foam and Cu foil) are applied with the same voltage since they are connected in parallel. However, the bottom end of copper foil undergoes the higher voltage than nickel foam since the copper foil has a lower resistance than the Ni foam, leading to the formation of a micro two-electrode electrochemical system. In this system the dissolved Cu^{2+} at Cu electrode will be reduced on the surface of Ni cathode to form copper oxide nanoparticles. Meanwhile, the electrons in the plasma can recombine with metallic ions to form metallic nanoparticles, similar to the reduction of metal ions by an electron beam [47].

Physical sputtering process: Since the plasma discharge zone of Cu foil overlaps that of Ni foam, the CuO particles will adhere easily to Ni foam surface with the assistance of the explosive force at the high temperature in the plasma discharge region and H_2 bubbles destabilization whilst the surface Ni foam also will be partially melt and form NiO nano-rods over the surface (Fig.s5). The melted CuO particles and NiO particles are incorporated together in the high temperature plasma region forming a number of nucleation sites for the growth of nanowires.

The nanowire growth process is started up as soon as the plasma discharge stop. As the surface temperature reduces, the compound nano-wires were found to slowly grow driven by the energy diffusion and charge transfer of the particles on the Ni foam surface. It may be that the electron collisions with molecules create highly reactive growth precursors, making the nano-wires growth largely irreversible and driving the reactions at low temperatures [48]. Nucleation and crystal growth, affecting by the liquid plasma, are different from those of the conventional thermal method. It is believed that the high electron temperature and the strong oxidizing agents generated by the liquid plasma discharge play an important role in the formation of the 3D nest-like structure electrode.

4. Conclusions

In summary, the double cathodes liquid plasma discharge is electrochemical physical process, including electrochemical deposition process and physical sputtering process. In the present work, this method was used to fabricate high efficiency 3D nest-like in-plane epitaxial structure electrode. As a catalyst, this 3D bimetal pure oxide achieves the excellent OER performance. It drives the current density to be 10 mA/cm^2 for CuO-NiO/NF electrode at an overpotential of 319 mV, which is lowered than 370 mV required for $Cu(OH)_2$-Ni_2O_3H/NF electrode. The much higher ECSA of the CuO-NiO/NF electrode (i.e.153 cm^2) than $Cu(OH)_2$-Ni_2O_3H/NF electrode (i.e. (63 cm^2) is partially responsible for the better performance. The coplanar growth of Cu and Ni oxides gives rise to a number of interfaces, which are not fully epitaxial and contain a lot of defects that provide effective paths for the fast transportation of charges. The double cathodes liquid plasma discharge technique reported in the present paper brings out an effective way to design and deliver a variety of desirable 3D porous electrodes upon request.

Conflict of interest

The authors declare that they have no conflict of interest.

Acknowledgements

This work was supported by Tier1 (AcRF grant MOE Singapore M4011959 and M4011528), Chinese Natural Science Foundation of China (Nos. 51271031 and 51771027) and the National Basic Research Program of China (No. 2014CB643300).

Appendix A. Supplementary data

Supplementary material related to this article can be found, in the online version, at doi:https://doi.org/10.1016/j.apcatb.2018.11.046.

References

[1] T.N. Huan, G. Rousse, S. Zanna, I.T. Lucas, X. Xu, N. Menguy, V. Mougel, M. Fontecave, Angew. Chemie 56 (2017) 4792–4796.
[2] B.K. Kim, S.-K. Kim, S.K. Cho, J.J. Kim, Appl. Catal. B-Environ. 237 (2018) 409–415.
[3] J. Zhang, H. Ma, Z. Liu, Appl. Catal. B-Environ. 201 (2017) 84–91.
[4] X. Li, X. Hao, A. Abudula, G. Guan, J. Mater. Chem. A 4 (2016) 11973–12000.
[5] Y.Ga.T.F. Jaramillo, J. Am. Chem. Soc 132 (2010) 13612–13614.
[6] L. Wang, H. Chen, Q. Daniel, L. Duan, B. Philippe, Y. Yang, H. Rensmo, L. Sun, Adv. Energy Mater. 6 (2016) 1600516.
[7] X. Zhao, X. Li, Y. Yan, Y. Xing, S. Lu, L. Zhao, S. Zhou, Z. Peng, J. Zeng, Appl. Catal. B-Environ. 236 (2018) 569–575.
[8] H. Chen, S. Ouyang, M. Zhao, Y. Li, J. Ye, ACS Appl. Mater. Interfaces 9 (2017) 40333–40343.
[9] G. Li, P.Y.A. Chuang, Appl. Catal. B-Environ. 239 (2018) 425–432.
[10] J. Wang, L. Ji, S. Zuo, Z. Chen, Adv. Energy Mater. 7 (2017) 1700107.
[11] X. Liu, H. Zheng, Z. Sun, A. Han, P. Du, ACS Catal. 5 (2015) 1530–1538.
[12] M. Yao, N. Wang, W. Hu, S. Komarneni, Appl. Catal. B-Environ. 233 (2018) 226–233.
[13] M.K. Bates, Q. Jia, H. Doan, W. Liang, S. Mukerjee, ACS Catal. 6 (2016) 155–161.
[14] M. Gao, W. Sheng, Z. Zhuang, Q. Fang, S. Gu, J. Jiang, Y. Yan, J. Am. Chem. Soc. 136 (2014) 7077–7084.
[15] X. Xu, F. Song, X. Hu, Nat. Commun. 7 (2016) 12324.
[16] A. Sivanantham, S. Shanmugam, Appl. Catal. B-Environ. 203 (2017) 485–493.
[17] Z. He, J. Fu, B. Cheng, J. Yu, S. Cao, Appl. Catal. B-Environ. 205 (2017) 104–111.
[18] H. Chen, Y. Gao, L. Sun, ChemSusChem 10 (2017) 1475–1481.
[19] L. Wang, X. Ge, Y. Li, J. Liu, L. Huang, L. Feng, Y. Wang, J. Mater. Chem. A 5 (2017) 4331–4334.
[20] J. Du, Z. Chen, S. Ye, B.J. Wiley, T.J. Meyer, Angew. Chemie 54 (2015) 2073–2078.
[21] S.M. Pawar, B.S. Pawar, B. Hou, J. Kim, A.T. Aqueel Ahmed, H.S. Chavan, Y. Jo, S. Cho, A.I. Inamdar, J.L. Gunjakar, H. Kim, S. Cha, H. Im, J. Mater. Chem. A 5 (2017) 12747–12751.
[22] X. Zhang, X. Cui, Y. Sun, K. Qi, Z. Jin, S. Wei, W. Li, L. Zhang, W. Zheng, ACS Appl. Mater. Interfaces 10 (2018) 745–752.
[23] B. Zhang, C. Li, G. Yang, K. Huang, J. Wu, Z. Li, X. Cao, D. Peng, S. Hao, Y. Huang, ACS Appl. Mater. Interfaces 10 (2018) 23807–23812.
[24] G. Wang, R. van den Berg, C. de Mello Donega, K.P. de Jong, P.E. de Jongh, Appl.

Catal. B-Environ. 192 (2016) 199–207.
[25] M.B. Gawande, A. Goswami, F.X. Felpin, T. Asefa, X. Huang, R. Silva, X. Zou, R. Zboril, R.S. Varma, Chem. Rev. 116 (2016) 3722–3811.
[26] J.Y.C. Chen, J.T. Miller, J.B. Gerken, S.S. Stahl, Synth. Lect. Energy Environ. Technol. Sci. Soc. 7 (2014) 1382.
[27] X. Lu, C. Zhao, Nat. Commun. 6 (6616) (2015) 6611–6617.
[28] N. Cheng, Y. Xue, Q. Liu, J. Tian, L. Zhang, A.M. Asiri, X. Sun, Electrochim. Acta 163 (2015) 102–106.
[29] C.C. Hou, C.J. Wang, Q.Q. Chen, X.J. Lv, W.F. Fu, Y. Chen, Chem. Commun. (Camb.) 52 (2016) 14470–14473.
[30] S.K. Sen Gupta, R. Singh, Plasma. Sour. Sci. T 26 (2016) 015005.
[31] A. Allagui, A.E. Rojas, T. Bonny, A.S. Elwakil, M.A. Abdelkareem, J. Appl. Phys. 119 (2016) 203303.
[32] H.-R. An, S.Y. Park, J.Y. Huh, H. Kim, Y.C. Lee, Y.B. Lee, Y.C. Hong, H.U. Lee, Appl. Catal. B-Environ. 211 (2017) 126–136.
[33] G. Saito, Y. Nakasugi, T. Yamashita, T. Akiyama, Nanotechnology 25 (2014) 135603.
[34] A. Allagui, T. Salameh, H. Alawadhi, Int. J. Enery.Res. 39 (2015) 1689–1697.
[35] D. Mariotti, R.M. Sankaran, J. Phys. D Appl. Phys. 43 (2010) 323001.
[36] M. Zhao, W. Yuan, C.M. Li, J. Mater. Chem. A 5 (2017) 1201–1210.
[37] W. Yuan, M. Zhao, J. Yuan, C.M. Li, J. Power Sour. 319 (2016) 159–167.
[38] M. Lee, H.S. Oh, M.K. Cho, J.P. Ahn, Y.J. Hwang, B.K. Min, Appl. Catal. B-Environ. 233 (2018) 130–135.
[39] R. Wüthrich, P. Mandin, Electrochim. Acta 54 (2009) 4031–4035.
[40] A.M.Ma.C. Greaves, J. Solid State Chem. 71 (1987) 418–425.
[41] S. Cui, X. Liu, Z. Sun, P. Du, ACS Sustain, Chem. Eng. 4 (2016) 2593–2600.
[42] X. Zhang, J. Qin, Y. Xue, P. Yu, B. Zhang, L. Wang, R. Liu, Sci. Rep. 4 (2014) 4596.
[43] X. Zhang, Y. Zhao, C. Xu, Nanoscale 6 (2014) 3638–3646.
[44] G.C. da Silva, N. Perini, E.A. Ticianelli, Appl. Catal. B-Environ. 218 (2017) 287–297.
[45] J. Chang, Q. Lv, G. Li, J. Ge, C. Liu, W. Xing, Appl. Catal. B-Environ. 204 (2017) 486–496.
[46] R. Wuthrich, A. Allagui, Electrochim. Acta 55 (2010) 8189–8196.
[47] J. Kugai, T. Moriya, S. Seino, T. Nakagawa, Y. Ohkubo, H. Nitani, Y. Mizukoshi, T.A. Yamamoto, Appl. Catal. B-Environ. 126 (2012) 306–314.
[48] Z. Wang, Y. Zhang, E.C. Neyts, X. Cao, X. Zhang, B.W.L. Jang, C.J. Liu, ACS Catal. 8 (2018) 2093–2110.